stellarator news

Published by Fusion Energy Division, Oak Ridge National Laboratory
Building 9201-2; P.O. Box 2009; Oak Ridge, TN 37831-8071, USA

Editor: James A. Rome Issue #9 May, 1990

Available Literature

Three collections of papers on recent stellarator studies of general interest are available.

The January 1990 issue of *Fusion Technology* (205 pages) was devoted to the status of new medium-size stellarator experiments that began operation in 1988, those scheduled to start in 1990–1991, and the large next-generation stellarators now under design that would start operation in the late 1990s.

The *Proceedings of the First International Toki Conference on Plasma Physics and Controlled Fusion* are available from the National Institute for Fusion Science (Nagoya, Japan) as report NIFS-PROC-3 (285 pages).

The *Proceedings of the Seventh International Stellarator Workshop*, held at Oak Ridge, TN, USA, in April 1989, will be distributed this month as an IAEA TECDOC report (about 570 pages).

In addition, a paper in the September 1990 issue of Nuclear Fusion will describe recent studies in the world stellarator community, the status of new and planned devices, theoretical studies, and large next-generation devices.

Next Issue Due Date

Please submit material for the July issue of *Stellarator News* to the Editor by June 20. The Editor also has another E-mail address to receive items from Internet: ROMEJA@ORNL.GOV.

H-1 Heliac

Construction of the H-1 heliac at the Australian National University in Canberra is proceeding apace. The main (36-turn) poloidal field coil, which links the 36 toroidal field coils, has been successfully wound in situ and is being encapsulated inside its vacuum jacket, prior to fitting of the surrounding 4-turn helical control winding. The whole coil set, including the two inner vertical field coils, will then be assembled onto its impressive-looking polished stainless steel support structure, the toroidal field coils being located in their helical positions according to their magnetically measured centers and axes. Final vertical and poloidal coil positions will be adjusted after the whole coil assembly is loaded inside its vacuum tank to allow e-beam field measurements to be made. This is expected to occur in the latter half of 1990.

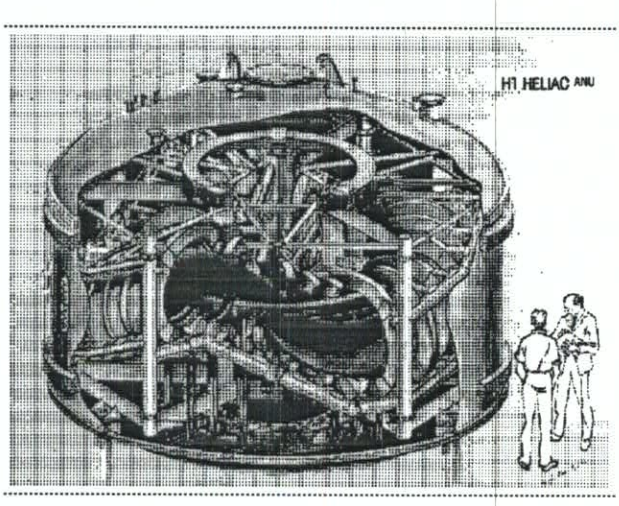

The H-1 Heliac being built at ANU

Around the Labs

News from Heliotron E

Recent experimental results are summarized as follows:

Confinement

The rotational transform, shear, average plasma radius a_p, and hill or well configuration are controlled by applying toroidal B_t and vertical B_v fields in addition to the helical field B_h. The two parameters, α^* ($\equiv B_t/B_h$) and β^* ($\equiv B_v/B_h$), change from –0.1 to 0.15 and from –0.198 to –0.172, respectively. The dependence of the gross energy confinement time τ_E^G on α^* and β^* has been analyzed by a 1-D profile analysis transport code (PROCTOR-Mod) with spatially resolved electron density, electron temperature, and ion temperature data. If α^* was increased from –0.1 to 0.15, the electron density increased from 2×10^{13} cm^{-3} to 6×10^{13}cm^{-3}, and the profile changed from peaked to broad, with the same gas puff conditions. The electron temperature ($T_e(0) \approx 500$ eV) and its profile were almost the same in the α^* scan. The ion temperature decreased from 700 eV to 500 eV. The optimum values of $W_p = 16$ kJ, $\tau_E^G = 9$ ms, and $n_e(0)\,\tau_E^G\,T_i(0) = 3.5 \times 10^{14}cm^{-3}\cdot$ s·eV for 2 MW port-through NBI power were obtained at α^*=0.05 and $\beta^* = -0.192$. The particle confinement time τ_p estimated by laser-induced H_α fluorescence and emission spectroscopy has also revealed behavior similar to that of τ_E^G. The average plasma radius changed as α^* increased, and it was found that the scaling of τ_E^G with size was consistent with an a^2 dependence. As α^* becomes larger than ≈0.08, the plasma-wall interaction becomes strong, and emissions of metallic impurities, such as iron, nickel, and chromium, increase drastically. The density ratio of iron to oxygen was estimated to be in the range from 1/50 to 1/100 using VUV spectroscopy.

Stability

Internal disruptions appeared on the soft X-ray signals with $\Delta I_{SX}/I_{SX}$ reaching a maximum of 60%. The inversion radius was close to $\iota = 2/3$ at $\alpha^* = -0.1$, and $\iota = 1/2$ for $\alpha^* \geq 0$. $m = 2, n = 1$ oscillations were found during two successive internal disruptions. For $\alpha^* \simeq 0.03 - 0.08$, these internal disruptions were stabilized. Low-frequency (8 – 20 kHz) m/n = 1/1, 2/1, 2/3 fluctuations, which are considered resistive interchange modes, were observed by magnetic probes. These instabilities were also stabilized at $\alpha^* \sim 0.05$.

Machine status

Heliotron E is not operating at present to allow the installation of two sets of inside ECH lauching systems and a 106-GHz, 500-kW gyrotron system. The main vacuum chamber will be evacuated again at the beginning of June. The next experimental phase will begin at the end of June. The electric potential will be measured by a heavy neutral beam probe (HNBP) for studying the relation of transport properties to the electric field.

Fraunhofer diffraction method for measuring density fluctuation

For measuring density fluctuations in the frequency range up to 400 kHz, the Fraunhofer diffraction method with a 50-W cw CO_2 laser beam ($\lambda = 10.6$ μm) is used. The essential point is that the mixing signal of the scattered light due to density fluctuation and the nonperturbed incident beam is detected. Thus, only one pair of ports opposite to each other is necessary for one chordal observation, which is adequate for the Heliotron E configuration. By detecting the mixed beam profile perpendicular to the laser beam, the Fraunhofer diffraction profile in the $k_\perp$ direction (k is the wave number, and ⊥ denotes the direction perpendicular to the magnetic field line) can be obtained. An example of a Fraunhofer diffraction profile is shown in Fig.1. The points are measurements, and the solid lines are fitted theoretical curves with k adjusted for each frequency. With this system, preliminary measurements of density fluctuations have been obtained. We have looked at the

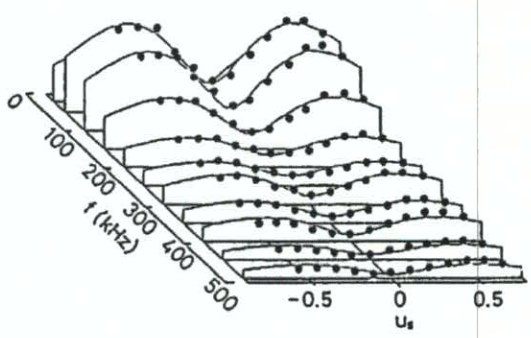

Fig. 1. Example of Fraunhofer diffraction profile

frequency (0–400 kHz) and wave number ($k_\perp \lesssim 1.5\ mm^{-1}$) fluctuation spectra, and they roughly agree with those expected for drift waves.

FIR Thomson scattering for ion temperature measurement

We are developing a new method of ion temperature measurement using far-infrared collective Thomson scattering with a D_2O laser ($\lambda = 385\ \mu m$). A pulsed single-mode CO_2 laser for pumping the D_2O laser has been constructed and has achieved high power at $\lambda = 9.26\ \mu m$, which is efficient for pumping the D_2O laser. From the viewpoint of obtaining an adequate signal-to-noise ratio, the D_2O laser must produce 200 kW of output power with a pulse duration longer than 1 μs. To achieve this, a CO_2 laser energy of more than 60 J with a pulse width longer than 1 μs is required. The wave form of the pumping CO_2 laser operated with the injection locking technique is shown in Fig. 2(a). The energy achieved is more than 80 J. TheD_2O laser waveform is shown in Fig. 2(b). The D_2O laser is at present operating in a multimode configuration. This point should be improved by the better resonator configuration obtained with a hybrid (cw and pulsed) CO_2 laser system.

Shigeru Sudo
Kyoto Plasma Physics Laboratory
Kyoto University
Kyoto, Uji, Japan

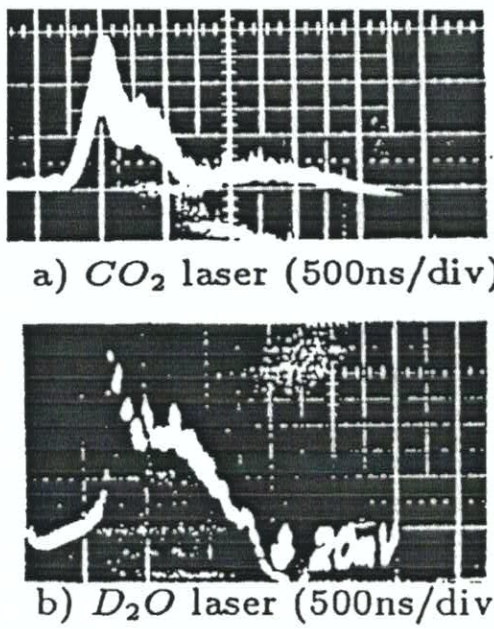

Fig. 2. Laser waveforms

Status of CHS

CHS was shut down for about three months (from the end of December 1989 to March 1990) for maintenance and overhaul of the flywheel motor generator. During this period, we made the second series of field mapping experiments and installed graphite armor plates and some new diagnostics.

In June 1988, when CHS was starting its experiments, the vacuum magnetic field structure was measured with an electron gun and a fluorescent mesh. We measured a small island at the $\iota = 1/2$ magnetic surface the size of which scaled in proportion to $B^{-1/2}$. We did not investigate the island at the $\iota = 1$ magnetic surface because the dc power supplies were not large enough to provide full control of the poloidal field. The objectives of the mapping experiments this spring are (1) to confirm that the $\iota = 1/2$ island size has not changed after the installations of numerous components around the torus since the time of the first field mapping experiments, (2) to observe the $\iota = 1$ magnetic surface which occurs near the outermost magnetic surface, and (3) to try the method of impedance measurements with an electron emitter for the first time in CHS.

It has been confirmed that the size of the $\iota = 1/2$ magnetic island is the same as it was two years ago. We also measured the $\iota = 1$ island this time; it is larger than $\iota = 1/2$ island but still has a clear boundary without ergodization. The impedance measurements with an electron emitter showed continuously decreasing conductivity when the emitter was moved to the center of magnetic surfaces. We observed the plateau region of the conductivity variation which corresponds to the islands observed in the fluorescent measurements.

Graphite armor plates were installed in CHS to achieve long-pulse operation of neutral beam heating experiments. Two curved plates were attached to the inboard side wall to protect it against the shinethrough of the beam when the beam injection angle approaches perpendicular. Another plate is installed on the side wall of the beam inlet port, which enables us to make longer beam pulses. We have been limiting the duration of the beam to 250 ms so far, but we are planning to extend it in the new series of experiments. The preliminary experiments of swinging the beam injector were done during the last year using a short pulse period (30 ms). Full operation for different beam injection angles is also scheduled.

Analyses of experimental data obtained in the last year have been done. Transport analysis was performed for both ECH- and NBI-heated plasmas using the code

PROCTR-Mod developed at ORNL. The data we used as input for the code are the electron density and temperature profiles measured with the Thomson scattering system, the ion temperature profile measured with charge-exchange recombination spectroscopy (for NBI plasmas), and the radiation profile measured with pyroelectric detectors. It was clear that the position of the temperature peak is shifted from that of vacuum field magnetic axis, especially for high-density NBI-heated plasmas. Equilibrium magnetic configurations are calculated using the VMEC code with measured pressure profiles.

The heat deposition profiles are determined by model calculations for both ECH and NBI plasmas. For the ECH case, it is assumed that the deposition is proportional to the electron cyclotron resonance region volume. The NBI deposition is calculated by PROCTR-Mod as the fast-ion birth profile. The electron heat conductivities for various plasma parameters are obtained in the range of 1–10 $m^2 \cdot s^{-1}$. When the magnetic field or the plasma density is increased, the heat conductivity decreases. These experimentally obtained conductivities are larger than the simple neoclassical prediction for both ECH and NBI cases by factors of 4 to 50. The profiles of radial electric field are obtained for NBI-heated plasmas using the data from charge-exchange recombination spectroscopy.

The electric field is estimated from the poloidal rotation speed profile and the ion temperature profile obtained from the Doppler shifts of charge-exchanged carbon ions. The poloidal rotation speed at the region near the plasma boundary (r/a = 0.8–0.9) is 5–10 km/s for the NBI plasma with the density 2–4 x 10^{13} cm^{-3}. It is faster for higher density plasma. The radial electric field is negative over all the plasma radius and larger at the plasma edge (70–110 V/cm).

Machine operation resumed in April. After one week of experiments, we achieved an 800-ms NBI plasma (tangential injection) without a radiation collapse for 1-T operation. The following experiments are scheduled: the plasma-surface interaction study with the graphite limiter, confinement study with variable beam injection angle, poloidal field control (vertical and quadrupole), precise transport study, etc.

Shoichi Okamura
National Institute for Fusion Science
464-01 Nagoya, Japan

Status of ATF

While the ATF is shut down for a high-voltage buswork upgrade and miscellaneous device and diagnostics tasks requiring a vacuum opening, we have been analyzing data and resolving several issues. In this article we report on changes in calibrations of NBI power and FIR interferometer data and their implications on confinement.

With the neutral beam power calibrations, corrected values of the injected power are about 75% of the old values. For example, the injection power used for the second stability experiment in September 1989 [1] was 1.1 MW instead of 1.4 MW, which was quoted in the reference. The highest power injected thus far is 1.5 MW.

There has been significant progress in understanding the FIR interferometer data. The discrepancy between line-averaged electron density values from the FIR interferometer and the 2-mm interferometer is now attributed to an unintentional shift of the FIR laser wavelength (185 μm rather than 215 μm). The correction results in an increase in $\bar{n}_e$ by 15% in the previous NBI data at high densities where the FIR data were used. Ray tracing calculations showed that a relatively large signal in the outermost detector was substantially due to deflection of the FIR laser beam in the sharp density gradient at the plasma edge. Taking account of the deflection of the beam results in a profile with less edge gradient, but most profiles measured thus far are still very broad. An automatic fringe counting routine has been implemented for FIR data analysis (with about 70% success rate even for rather poor signal quality). This will speed up the data analysis and also make NBI experiments more efficient by feeding back the information during operation.

With these changes in calibrations of NBI power and FIR density measurements, values of both confinement time and density have increased. The highest confinement times are about 30 ms (20 ms) with 0.7 MW (1.4 MW) injection, and they are about 20% higher than those previously quoted. Because stellarator (empirical) scalings already include the positive density dependence, the increase in confinement time does not change the fit of ATF data to the scalings. Specifically we note that both the LHD scaling and the gyro-reduced Bohm scaling still provide good fits to the ATF data.

Masanori Murakami for the ATF Group
Oak Ridge National Laboratory
P.O. Box 2009
Oak Ridge, TN 37831-8072

Whistler Waves Generate High Plasma Densities in SHEILA

One planned method of plasma production in the heliac H-1 (R/a $\approx$ 1.0 m/0.2 m, B $\approx$ 1.0 T, under construction at the Australian National University) is through the excitation of whistler (helicon) waves. In preparation for this, recent experiments of rf plasma production using whistler waves have been carried out on the prototype heliac SHEILA (R/a $\approx$ 0.2 m/0.03 m, B $\approx$ 0.2 T) at the Australian National University. Peak densities above 10^{19} m^{-3} in argon have been reached with a total available power not exceeding 3 kW at 7 MHz. The launching antenna is a 10-cm-long double loop with a helical twist. Straight double-loop antennas have been used previously in linear devices to efficiently generate plasma using whistler waves [1].

The propagation of whistler waves depends sensitively upon having the correct relation between antenna length, power input, filling pressure, and magnetic field. When these parameters satisfy a critical relationship for a resonant whistler mode, dramatic switching between high- and low-density modes is seen to occur. Figure 1 shows this for 1-kW power input, a filling pressure of 3×10^{-4} Torr, a peak magnetic field of 0.18 T, and a peak density of $\approx 10^{18} m^{-3}$. At slightly higher filling pressures only the high-density mode is observed.

To reach even higher densities, 1.2×10^{19} m^{-3}, the filling pressure is raised tenfold and the power increased to 3 kW. The additional ionization required to allow a high-density whistler mode to propagate, is provided by superimposing the standard weak (0.4 kW) ac current on to the core winding of SHEILA for the first 5 ms of a typical 30 ms rf pulse. The observed density depends strongly upon the instantaneous magnetic field, following the same temporal behavior as the magnetic field pulse. Figure 2 shows such a shot at 2 kW where a double-humped magnetic field pulse was used to show the dependence of density on the magnetic field. Favorable scaling with magnetic field in both linear devices and SHEILA and recent results of plasma production in CHS [2] using whistler waves provide promise for the extrapolation of these results to H-1.

[1] Peiyuan Zhu and R. W. Boswell, Phys. Rev. Lett. **63**, 2805 (1989).

[2] K. Nishimura et al, Nagoya University, IPP Annual Report, April 1988 – May 1989, 26.

Boyd Blackwell
Plasma Physics Laboratory
Australian National University
G.P.O. Box 4
Canberra, ACT 2601, Australia

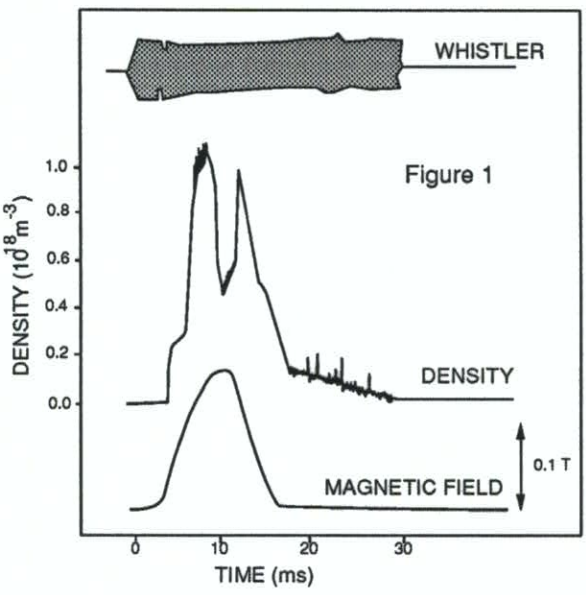

Fig. 1. Critical behavior of whistler mode in an experimental trace.

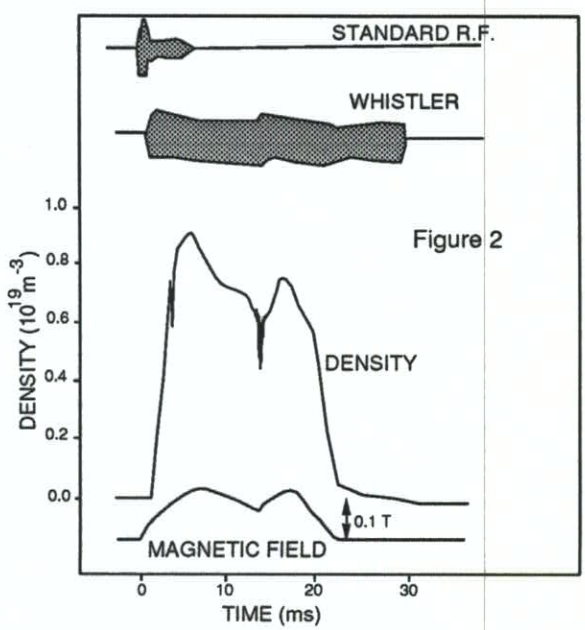

Fig. 2. SHEILA shot at higher filling pressures with standard rf added.